Theory of Stokes and anti-Stokes generation by Raman frequency conversion in the transient limit

A. P. Hickman and W. K. Bischel
Molecular Physics Department, SRI International, Menlo Park, California 94025
(Received 20 July 1987)

Analytic and numerical solutions are obtained for the equations describing the propagation of several pulses of different frequencies through a Raman medium. The transient case is treated, and the analysis includes Stokes, pump, and anti-Stokes frequency components. The effect of phase mismatch Δk between these waves is investigated. An analytic solution is found that describes the phenomenon of transient Stokes–anti-Stokes gain suppression in the limit $\Delta k=0$. For nonzero values of Δk, the behavior of the transient gain coefficient is found to follow a scaling rule that is the analog of a similar result known from the steady-state limit. Calculations are performed to identify conditions that enhance conversion to anti-Stokes radiation. It is found that there is an optimum strength of the Stokes seed, and that proper phase matching of the initial waves is essential.

I. INTRODUCTION

Raman scattering and frequency conversion in the propagation of laser pulses have been the subject of several recent theoretical papers.[1–5] Much of the work was stimulated by the observation of efficient conversion in H_2 of 560-nm pulses to higher-order anti-Stokes radiation.[6] Other recent experiments have revealed evidence of solitons[7] in Raman scattering, and this has led to a search for corresponding analytic solutions to the basic equations or Raman scattering in the extreme transient limit. A previous paper by the present authors,[3] denoted I, focused on the development of a theoretical approach that could handle higher-order frequency components and pulses strong enough to induce substantial excited-state molecular populations. This paper generalizes the investigation begun in I. The additional effect considered is the phase mismatch between different frequency components due to dispersion.

This paper examines several situations where this phase mismatch is important. The emphasis is on cases in which only Stokes, pump, and anti-Stokes pulses are large and the pulses are short compared to the relaxation time of the medium. We present several important new results. First, we have considered the phenomenon of gain suppression,[8,9] and have found an analytic solution for an important limiting case of the general equations that gives considerable insight into this process. Second, we have investigated the transient gain of small Stokes seed pulses as a function of the momentum mismatch. We find that we can describe a wide range of numerical results using a scaling rule that is completely analogous to one determined several years ago for the steady-state case by Bloembergen.[8] Finally, we have explored situations leading to a large conversion of energy to the first anti-Stokes pulse.

Section II presents the general form of our working equations. The analytic and numerical solutions we have obtained for a variety of situations are presented and discussed in Sec. III. Section IV contains concluding remarks.

II. GENERAL EQUATIONS

This section presents the equations describing the copropagation of pulses at several different frequencies through a Raman medium. As in I, we let the complex field envelope for the wave at frequency $\omega_n=\omega_0+n\omega_R$ be $V_n(z,t)$. Negative, zero, and positive integers n refer to the corresponding orders of Stokes, pump, and anti-Stokes waves, and t is the retarded time $t=t_{\rm lab}-z/c$. Coupled equations for the V_n are then

$$\frac{\partial V_n}{\partial z}=-i\,\Delta k_n\,V_n+\frac{\pi\rho\alpha_{12}\omega_n}{c}[(v-iu)V_{n+1}-(v+iu)V_{n-1}], \tag{1}$$

where u, v, and w are the solutions to the Bloch equations,

$$\frac{\partial u}{\partial t}=-\frac{u}{T_2}-\Delta v-\Omega_I w\ ,$$
$$\frac{\partial v}{\partial t}=\Delta u-\frac{v}{T_2}-\Omega_R w\ , \tag{2}$$
$$\frac{\partial w}{\partial t}=\Omega_I u+\Omega_R v-\frac{w-w_0}{T_1}\ ,$$

and

$$\Omega=\Omega_R+i\Omega_I=\frac{\alpha_{12}}{2\hbar}\sum_n V_n V_{n-1}^*\ , \tag{3}$$

$$\Delta=\delta\omega+\frac{\alpha_{22}-\alpha_{11}}{4\hbar}\sum_n V_n V_n^*\ . \tag{4}$$

Δ includes possible detuning and the ac Stark shift. The coupling constants α_{ij} are as defined in I.

Equations (1)–(4) differ slightly from the corresponding Eqs. (16)–(19) and (22) in I. The phase factor $\exp(-i\theta)$ in I has been eliminated by the coordinate rotation $(u+iv)$ (this paper) $=\exp(-i\theta)[(u+iv)]$ (paper I). The angle θ is defined by $|\Omega|\exp(i\theta)=\Omega_R+i\Omega_I$. The rotation modifies the detuning Δ, which in this paper does not include the term $\partial\theta/\partial t$ as it did in I.

Equation (1) also generalizes Eq. (22) of I by including the momentum mismatch terms Δk_n, which are defined in Fig. 1. We effectively consider the z components of waves propagating in directions $\mathbf{k}_n$, and neglect transverse derivatives in the Maxwell wave equation. This approximation should be reasonable for small cone angles θ_n, as long as there is good spatial overlap between the interacting waves. In the absence of coupling between the waves ($\alpha_{12}=0$) a solution to Eq. (1) for V_n is $\exp(-i\Delta k_n z)$, corresponding to a physical field given by

$$E_n(z,t_{\rm lab})=\exp(-i\Delta k_n z)\exp[i\omega_n(t_{\rm lab}-z/c)]$$
$$=\exp\left\{i\left[\omega_n t_{\rm lab}-\left[\frac{\omega_n}{c}+\Delta k_n\right]z\right]\right\}. \quad (5)$$

This result shows that the uncoupled waves would have wave vectors whose z components were $k_n\cos\theta=(\omega_n/c)+\Delta k_n$, as shown in Fig. 1. The values of k_n are determined by assuming that the index of refraction of the medium does not change when the pulse excites some of the molecules. Then

$$k_n=\frac{\omega_n}{c}(1+4\pi\rho\alpha_{11})^{1/2}, \quad (6)$$

where ρ is the molecular number density and the square-root factor is the index of refraction.

Equations (1) and (2), our current working equations, are solved directly. Arbitrary values of the momentum mismatches Δk_n may be selected. The maximum orders of Stokes and anti-Stokes fields are limited by storage capability. We have routinely handled nine wave calculations ($n=-4,-3,\ldots,+4$). The numerical technique is to solve a larger set of coupled, z-dependent, first-order ordinary differential equations for the real and imaginary parts of $V_n(z,t_m)$ at a set of times t_m. Typically, 100–400 time steps are used. The number of time steps and the number of fields together determine the size of the program.

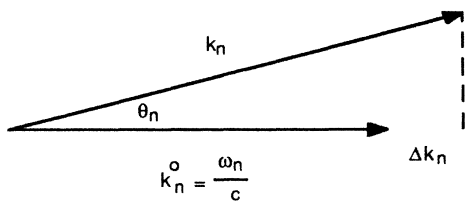

FIG. 1. The momentum mismatch $\Delta k_n=k_n\cos\theta_n-\omega_n/c$ arises because the z component of the wave vector $\mathbf{k}_n$ differs from the value $k_n^0=\omega_n/c$ that characterizes propagation on axis in a dispersionless medium. The diagram is not to scale. For the situations considered in this paper, k_n is larger than k_n^0 by a few parts in 1000, and the θ_n are a few milliradians.

It is illustrative to transform Eqs. (1) and (2) to a form that more clearly exhibits the role of the momentum mismatch terms Δk_n. If we define

$$F_n(z,t)=\exp(i\,\Delta k_n)V_n(z,t) \quad (7)$$

then the F_n satisfies the following coupled equations:

$$\frac{\partial F_n}{\partial z}=\frac{\pi\rho\alpha_{12}\omega_n}{c}(e^{-i\Delta_{n+1}z}q^*F_{n+1}-e^{i\Delta_n z}qF_{n-1}), \quad (8)$$

where the complex variable

$$q=\exp[i(\Delta k_0-\Delta k_{-1})z](v+iu) \quad (9)$$

is the solution to a set of Bloch equations, and Δ_n is a composite momentum mismatch given by

$$\Delta_n=\Delta k_n-\Delta k_{n-1}-(\Delta k_0-\Delta k_{-1}). \quad (10)$$

We can recover a simple form of the equations of Raman scattering by considering only $n=-1,0,1$ (Stokes, pump, and anti-Stokes waves), assuming that very few atoms are excited by the laser pulses, and solving the Bloch equations analytically for the limit $w=-1$,

$$\frac{\partial F_{-1}}{\partial z}=\frac{\pi\rho\alpha_{12}\omega_{-1}}{c}q^*F_0,$$
$$\frac{\partial F_0}{\partial z}=\frac{\pi\rho\alpha_{12}\omega_0}{c}(e^{-i(\Delta k)z}q^*F_1-qF_{-1}), \quad (11)$$
$$\frac{\partial F_1}{\partial z}=-\frac{\pi\rho\alpha_{12}\omega_1}{c}e^{i(\Delta k)z}qF_0,$$

where

$$q=\frac{\alpha_{12}}{2\hbar}\int_{-\infty}^{t}\exp\left[-\frac{t-t'}{T_2}\right](e^{-i(\Delta k)z}F_1F_0^*+F_0F_{-1}^*)dt' \quad (12)$$

and

$$\Delta k=\Delta_1=\Delta k_1-2\,\Delta k_0+\Delta k_{-1}. \quad (13)$$

We can perform the calculations for arbitrary values Δk_n, but our model does not specify these values. For the case of three coupled waves, only the composite momentum mismatch Δk is important, and we have explored the effect of a range of values of this parameter. For calculations involving higher-order waves, we have adopted a method derived from the work of Brink and Proch[10] to specify the Δk_n. The angles θ_{-1} and θ_1 may be determined for perfect phase matching ($\Delta_1=\Delta k=0$) by considering Fig. 2. One can then work upward through the anti-Stokes waves ($n\geq 1$) by assuming θ_{n-1} is known, and then choosing θ_n to minimize $|\Delta\mathbf{k}_n|$, where

$$\Delta\mathbf{k}_n=\mathbf{k}_n-\mathbf{k}_{n-1}-\mathbf{k}_0+\mathbf{k}_{-1}. \quad (14)$$

The result is

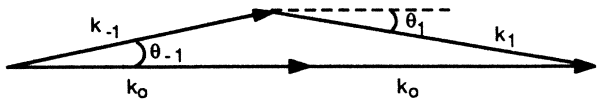

FIG. 2. Vector coupling diagram used for the determination of the angles for perfect phase matching of pump (k_0), Stokes (k_{-1}), and anti-Stokes (k_1) wave vectors.

$$\tan\theta_n=\frac{k_{-1}\sin\theta_{-1}+k_{n-1}\sin\theta_{n-1}}{k_0+k_{n-1}\cos\theta_{n-1}-k_{-1}\cos\theta_{-1}} . \tag{15}$$

Similarly, one can work downward ($n\leq -1$). Assuming θ_n is known, θ_{n-1} is chosen to minimize $|\Delta\mathbf{k}_{n-1}|$. The result is

$$\tan\theta_{n-1}=\frac{k_{-1}\sin\theta_{-1}+k_n\sin\theta_n}{k_{-1}\cos\theta_{-1}+k_n\cos\theta_n-k_0} . \tag{16}$$

The z component of the right-hand side of Eq. (14) is exactly the composite momentum mismatch obtained in Eq. (10). Another possible prescription would be to choose the cone angles θ_n to minimize the z component of $\Delta\mathbf{k}_n$. For the present application, the cone angles are a few milliradians, and the difference is negligible. However, in general, further study is needed to resolve the point.

III. ANALYTIC AND NUMERICAL SOLUTIONS

A. Analytic solution for transient Stokes–anti-Stokes gain suppression

Let us consider the form of Eqs. (11) and (12) for the special case of negligible pump depletion [$F_0=F_0(t)$]. Then we may write

$$\begin{aligned}\frac{\partial F_{-1}}{\partial z}&=\frac{\pi\rho\alpha_{12}\omega_{-1}}{c}q^*F_0 ,\\ \frac{\partial F_1}{\partial z}&=-\frac{\pi\rho\alpha_{12}\omega_1}{c}e^{i(\Delta k)z}qF_0 ,\\ \frac{\partial q}{\partial t}&=-\frac{q}{T_2}+\frac{\alpha_{12}}{2\hbar}(e^{-i(\Delta k)z}F_1F_0^*+F_0F_{-1}^*) .\end{aligned} \tag{17}$$

The momentum mismatch Δk depends on the relative angles of propagation of the pump, Stokes, and anti-Stokes pulses. In an experiment in which a seed Stokes beam crosses a pump beam the relative angle of k_{-1} and k_0 is determined, and there is a correspondence between Δk and k_1, the cone angle at which the anti-Stokes light is generated. Recently, Duncan *et al.*[9] have performed such an experiment. They have measured the intensity of anti-Stokes generation as a function of cone angle, and can correlate a minimum in this intensity with the direction of k_1 corresponding to gain suppression for $\Delta k=0$.

The behavior of solutions to Eq. (17) depends critically on the value of Δk. We present in this section an analytic solution for the case $\Delta k=0$. For the other limiting value $\Delta k\rightarrow\infty$ the terms involving the rapidly oscillating exponential may be neglected and the analytic solution of Carman *et al.*[11] recovered. In Sec. III B a scaling formula will be determined numerically that gives the approximate behavior of the solution for intermediate values of Δk in terms of reduced variables.

We first quickly review the solution of Carman *et al.*[11] for $\Delta k\rightarrow\infty$. If we make the substitutions $\kappa_1=\alpha_{12}/(2\hbar)$, $\kappa_2=\pi\rho\alpha_{12}\omega_{-1}/c$, $\Gamma=1/T_2$, and $-iQ^*=q^*$ and set the rapidly oscillating exponentials to zero, Eq. (17) becomes

$$\begin{aligned}\frac{\partial F_{-1}}{\partial z}&=-i\kappa_2Q^*F_0 ,\\ \frac{\partial Q^*}{\partial t}&=-\Gamma Q^*+i\kappa_1F_{-1}F_0^* .\end{aligned} \tag{18}$$

In the extreme transient limit ($\Gamma=0$) and for the case that the seed Stokes pulse has the same shape as the pump pulse,

$$F_{-1}(0,t)=\gamma F_0(t) , \tag{19}$$

the analytic solution of Carman *et al.*[11] is

$$F_{-1}(z,t)=\gamma F_0(t)I_0(2\sqrt{\kappa_1\kappa_2z\tau}) , \tag{20}$$

where

$$\tau(t)=\int_{-\infty}^{t}F_0(t')^2dt' . \tag{21}$$

We have found that Eq. (17) may be solved analytically for $\Delta k=0$ and for $\Gamma=0$, if $F_0(t)$ is real and if Eq. (19) is assumed. In this case F_{-1}, F_1, and $q=iQ$ are real, and the substitution $G=F_1+F_{-1}$ transforms Eq. (17) to

$$\begin{aligned}\frac{\partial G}{\partial z}&=-i\kappa_2(1-\omega_1/\omega_{-1})Q^*F_0 ,\\ \frac{\partial Q^*}{\partial t}&=i\kappa_1GF_0 .\end{aligned} \tag{22}$$

This is exactly the same form as Eq. (18) for $\Gamma=0$, with the exception that the factor $(1-\omega_1/\omega_{-1})$ is negative. Therefore, the solution is

$$G(z,t)=\gamma F_0(t)J_0[\beta(z,t)] , \tag{23}$$

where

$$\beta(z,t)=2\{[(\omega_1/\omega_{-1})-1]\kappa_1\kappa_2z\tau\}^{1/2} . \tag{24}$$

We have used the general relation[12] that $I_0(ix)=J_0(x)$. By using analytic formulas for integrals over Bessel functions[12] it is easily shown that

$$Q^*(z,t)=\frac{i\gamma\kappa_1\tau}{\beta(z,t)}J_1(\beta(z,t)) . \tag{25}$$

Furthermore, the explicit solution for the fields is

$$\begin{aligned}F_{-1}(z,t)&=\gamma F_0(t)\frac{\omega_1}{2\omega_R}\left[1-\frac{\omega_{-1}}{\omega_1}J_0(\beta(z,t))\right] ,\\ F_1(z,t)&=-\gamma F_0(t)\frac{\omega_1}{2\omega_R}[1-J_0(\beta(z,t))] .\end{aligned} \tag{26}$$

This analytic solution gives considerable insight into the phenomenom of gain suppression. It is illustrative to consider the behavior of Eq. (26) in the limits of small

and large z. For $z \to 0$, we use the behavior of the Bessel function for small arguments (Ref. 12), $J_0(x) \cong 1 - x^2/4$, to obtain

$$F_{-1}(z,t) \cong F_{-1}(0,t)[1 + \kappa_1 \kappa_2 \tau(t) z + \cdots] ,$$
$$F_1(z,t) \cong F_{-1}(0,t) \left[-\frac{\omega_1}{\omega_{-1}} \kappa_1 \kappa_2 \tau(t) z + \cdots \right] . \quad (27)$$

This result clearly shows the initial behavior of the Stokes and anti-Stokes pulses. The Stokes pulse starts at the seed value, and grows. The anti-Stokes pulse is initially zero, and grows out of phase with the Stokes pulse. This phase difference is a crucial part of gain suppression. It leads to the decrease in the two-photon excitation rate.

As $z \to \infty$, $J_0 \to 0$ and the Stokes and anti-Stokes pulses approach limiting values for which the two fields are equal in magnitude and have opposite phase. The two-photon excitation rate is then zero. From Eq. (26) it is clear that the total final energy in each pulse is a factor $[\omega_1/(2\omega_R)]^2$ greater than the energy in the initial Stokes seed pulse. This is exactly the same behavior that is observed in the steady-state case.

We have therefore found contrasting behavior in two analytic solutions describing Stokes–anti-Stokes coupling in the transient regime. For perfect phase matching, $\Delta k = 0$, the seed Stokes pulse initially grows, but the growth is cut off as the anti-Stokes pulse is generated. As $z \to \infty$, both pulses approach a limiting form that is independent of z. For the opposite case that the anti-Stokes wave vector does not couple to the Stokes, the Stokes grows rapidly. We will illustrate these limiting cases, and intermediate situations, with numerical example in Sec. III B.

B. Stokes–anti-Stokes coupling

This section reports a series of calculations of the behavior of the Stokes and anti-Stokes pulses according to Eqs. (11)–(13). [Recall that the equations actually solved are the equivalent Eqs. (1) and (2).] We will consider Gaussian pulses that are short compared to the relaxation times T_2 of the medium, corresponding to the transient limit, although the numerical solutions nevertheless include the effect of finite T_2. We first present the results for specific values of the parameters chosen to correspond to typical laboratory experiments. Then we present a method for systematically representing the calculated behavior as a function of Δk, taking advantage of the behavior in the two limiting cases $\Delta k = 0$ and $\Delta k = \infty$ known analytically. The result of this analysis is a numerically determined scaling function that is the analog of a similar function determined earlier by Bloembergen[8] in the steady-state limit.

We now present specific calculations illustrating the effect of the momentum mismatch Δk on the growth of the Stokes and anti-Stokes waves. The Raman medium is taken to be H_2 at 10 amagat. For this example the pump (ω_0) has a wavelength of 193 nm, and the Raman transition is between the 0 and 1 vibrational levels (4155 cm^{-1}). The initial pump and seed pulse envelopes $F_0(0,t)$ and $F_{-1}(0,t)$ are proportional to $\exp[-(t/t_0)^2]$, with $t_0 = 0.100$ ns, corresponding to a full width at half maximum (FWHM) of 0.118 ns. The pump peak intensity was 1 GW/cm^2, and the seed peak intensity was a factor of 10^6 smaller. Relaxation times of $T_2 = 0.6$ ns and $T_1 = 1.2$ ns were used.

We present our numerical results in terms of the conversion efficiency as a function of the distance propagated through the medium. The energy in the pulse of frequency ω_n is

$$U_n(z) = \frac{c}{8\pi} \int_{-\infty}^{\infty} |F_n(z,t)|^2 dt . \quad (28)$$

The conversion efficiency to the nth frequency component is

$$\eta_n(z) = \frac{U_n(z)}{\sum_{n'} U_{n'}(0)} . \quad (29)$$

The numerical calculations account for the energy left behind the pulse in the form of excited molecules. Neglecting this term, which is very small for the intensities considered here, the conversion efficiencies for each wave correspond to the fraction of the total field energy in that wave.

The first panel of Fig. 3 shows the results when the anti-Stokes pulse is omitted from the calculation. The growth of the Stokes pulse is rapid until pump depletion occurs. The second panel shows the results for Stokes, pump, and anti-Stokes waves with perfect phase matching, $\Delta k = 0$. This calculation illustrates the phenomenon of gain suppression, which has been analyzed in the steady-state limit by Bloembergen.[8] We find the same qualitative behavior in the transient regime. The Stokes pulse is initially amplified, and the anti-Stokes pulse is generated. As the anti-Stokes pulse becomes larger, the growth of the Stokes pulse is suppressed. Asymptotically, both approach the same limiting, constant value.

The remaining panels of Fig. 3 show the numerical results for three wave calculations (Stokes, pump, and anti-Stokes) for successively larger values of Δk. As Δk increases, the long term growth of the Stokes pulse occurs more rapidly. For the largest values of Δk, the anti-Stokes pulse has little effect, and the behavior of the Stokes pulse is the same as if the anti-Stokes wave were completely neglected. This result confirms the assertion in Sec. III A that the rapidly varying exponential term $\exp[i(\Delta k)z]$ could be replaced by its average value, zero.

It is naturally of interest to try to predict the rate of growth of the Stokes (or anti-Stokes) pulse for a prescribed Δk. We address this question by noting that Carman's analytic solution for the two-wave case ($\Delta k \to \infty$), summarized in Sec. III A, gives the rate of growth of the energy in the Stokes pulse in the extreme transient limit ($T_2 \to \infty$). The result is

$$U_{-1}(z) = U_{-1}(0)[I_0(\beta_{\max}(z))^2 - I_1(\beta_{\max}(z))^2] , \quad (30)$$

where I_0 and I_1 are modified Bessel functions and

$$\beta_{\max}(z) = 2\sqrt{\kappa_1 \kappa_2 z \tau_{\max}} \quad (31)$$

and

$$\tau_{\max}=\int_{-\infty}^{\infty} F_0(t)^2 dt \ . \tag{32}$$

From the properties of Bessel functions[12] it can be shown that as $x \rightarrow \infty$

$$I_0(x)^2-I_1(x)^2 \rightarrow \frac{\exp(2x)}{2\pi x^2} \ , \tag{33}$$

and therefore

$$U_{-1}(z)=U_{-1}(0)\frac{2}{\pi}\frac{\exp[(z/z_0)^{1/2}]}{(z/z_0)} \ , \tag{34}$$

where

$$\frac{1}{z_0}=\frac{8\pi\rho\alpha_{12}^2\omega_{-1}}{\hbar c}\int_{-\infty}^{\infty} |F_0(t)|^2 dt \ . \tag{35}$$

This result suggests that we could characterize the growth of the Stokes pulse for an arbitrary Δk in terms of a transient gain coefficient $g(\Delta k)$, defined such that

$$U_{-1}(z) \propto \frac{1}{z}\exp[(g(\Delta k)z)^{1/2}] \ . \tag{36}$$

Clearly, in the limit $\Delta k=\infty$, $g(\Delta k)=1/z_0$. Furthermore, Eq. (36) implies that $\ln[zU_{-1}(z)]$ should be a linear function of $z^{1/2}$, with slope $[g(\Delta k)]^{1/2}$. We have found that such plots of our numerical results are indeed approximately linear, permitting us to estimate the function $g(\Delta k)$.

The ideal would be that $g(0)=0$, corresponding to the notion that the asymptotic behavior for perfect phase matching ($\Delta k=0$) is zero gain. However, substituting $g=0$ into Eq. (36) yields $U_{-1}(z)\sim 1/z$, which is not correct. [Eq. (26) predicts $U_{-1}(z) \rightarrow$ constant as $z \rightarrow \infty$.] Fortunately, Eq. (36) does appear to be a reasonable representation of our numerical results for rather small values of Δk, even though the actual limit does not behave correctly. Our viewpoint is that Eq. (36) still provides a very useful approximation to the behavior of the numerical calculations.

We have found that a useful way to represent the results of a wide variety of numerical calculations is to plot $g(\Delta k)/g(\infty)$ as a function of $\Delta k/g(\infty)$. This "universal" curve is shown in Fig. 4. Because the quantities plotted are dimensionless, the results obtained from specific calculations may be scaled to a wide range of other values of the parameters involved. For example, most of the results were obtained for a Stokes seed with the same shape of the pump pulse, and 10^{-6} of the intensity. Similar results are obtained for seed intensities 10^{-8} or 10^{-10} of the pump intensity. Similarly, a few calculations were tried in which the (still Gaussian) seed pulse had a narrower half-width than the pump, and was slightly displaced to the leading or trailing edge of the pump pulse. In these cases, the value of $g(\infty)$ must be explicity obtained from a calculation including only the Stokes and the pump pulse, because the analytic result $g(\infty)=1/z_0$ only applies for a Stokes pulse exactly proportional to the pump pulse.

The behavior represented in Fig. 4 presents a striking parallel to the results obtained in the steady-state limit by Bloembergen. Although the qualitative similarity of the

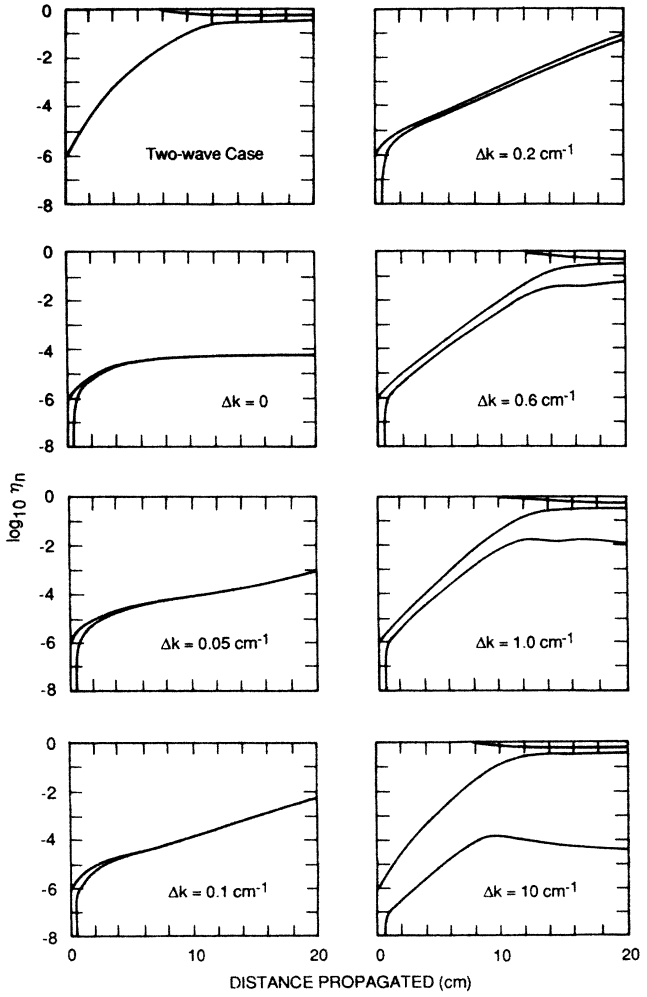

FIG. 3. The results of a series of calculations of the conversion efficiency $\eta_n(z)$ for different values of the momentum mismatch Δk. In each panel, the Stokes seed has the initial value $\eta_{-1}(0)=10^{-6}$; the pump has $\eta_0(0)\simeq 1$, and the anti-Stokes has $\eta_1(0)=0$.

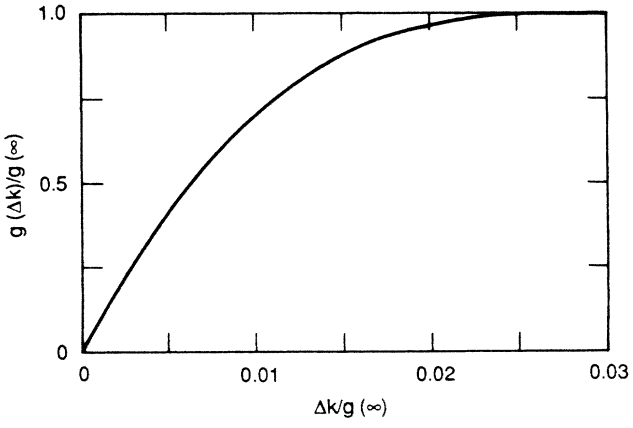

FIG. 4. Numerically determined behavior of the transient gain coefficient $g(\Delta k)$ describing the large-z behavior of calculations of the type presented in Fig. 3.

steady-state and transient solutions has been noticed, it is remarkable that the analog appears to be so complete.

C. Optimization of anti-Stokes conversion

This section describes a series of calculations designed to maximize the generation of light at the first anti-Stokes frequency. As in Sec. III B, the initial conditions will be a pump pulse at frequency ω_0 and a copropagating seed pulse at the Stokes frequency $\omega_{-1}=\omega_0-\omega_R$. The relative strength of the seed Stokes pulse will be varied to try to maximize the amount of energy in the generated anti-Stokes pulse. We will start with much stronger seed pulses than in Sec. III B, and we will follow their development through the stages of growth and pump depletion. For such calculations it appears that less use can be made of general scaling functions. Therefore, we report the results of several numerical calculations for specific values of the initial pulse characteristics.

We first present a series of calculations in which perfect phase matching is assumed ($\Delta k=0$), and the energy of the Stokes seed is varied. The pump (248 nm) and seed (276 nm) pulses are both Gaussian with FWHM of 0.589 ns ($t_0=0.5$ ns). The density of H_2 was 5 amagat, and the relaxation times were $T_2=1.0$ ns and $T_1=2.4$ ns. The pump peak intensity is held constant at 0.2 GW/cm^2, and the seed peak intensity is λ times this value. (The ratio of field envelopes is $\lambda^{1/2}$.) The calculation included three fields (pump, Stokes, and anti-Stokes), and the value of λ was varied from 10^{-3} to 10^{-1}. Figure 5 shows that the maximum conversion efficiency occurs at $\lambda=1.5\%$. The behavior of the conversion efficiency as a function of λ follows a simple curve related to the analytic results for the case of negligible pump depletion. This curve is also shown on the figure, and will be discussed in more detail below.

We also performed a series of calculations in which the seed pulse has 1.5% of the energy of the pump pulse, and in which the momentum mismatch Δk is varied. Other characteristics of the pulses were the same as for the calculation previously described. As shown in Fig. 6, the maximum conversion efficiency occurs for perfect phase matching, and the efficiency falls off rapidly as Δk increases.

The results of Fig. 6 present an interesting contrast with those of Sec. III B. For weak seed pulses ($\sim 10^{-6}$), perfect phase matching led to the minimum rate of growth of the Stokes and anti-Stokes pulses. For strong seed pulses (~ 1–2%), perfect phase matching leads to the maximum conversion of energy to the anti-Stokes wave. This behavior is less paradoxical than one might think. For the former case, pump depletion is not a factor, and the quantity considered is the rate of growth of the Stokes and anti-Stokes energy for large distances. Note, however, that for $\Delta k=0$ Eqs. (26) show that the level at which the Stokes and anti-Stokes pulse energies become constant corresponds to an amplification of the initial Stokes pulse by a factor of $[\omega_1/(2\omega_R)]^2$. This factor is 28.6 for an KrF laser (wavelength of 248 nm) and the 0-1 vibrational transition in H_2. Such an amplification of a 1.5% seed is not possible without substantial pump depletion. The generation of anti-Stokes light appears to be most effective when the initial waves are perfectly phase matched and an initial rapid generation and growth of the anti-Stokes wave occurs. Pump depletion then occurs before the asymptotic limit corresponding to our previous discussion of gain suppression comes into play. The condition $\Delta k=0$ is also consistent with Eqs. (11) and (17), which leads one to expect that the derivative of the anti-Stokes pulse will be largest, on average, when there are no oscillations from the exponential factor.

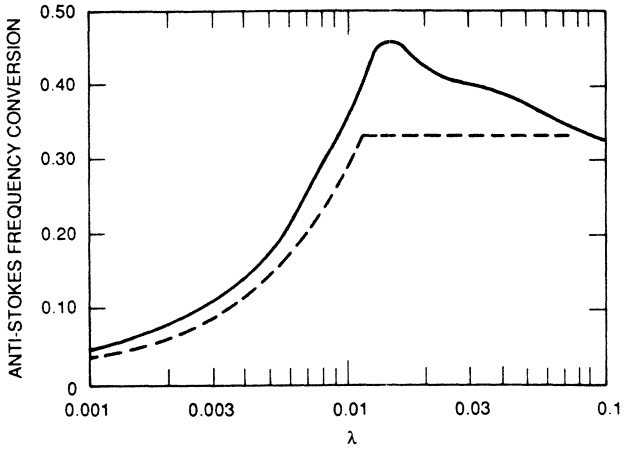

FIG. 5. Behavior of the anti-Stokes conversion efficiency as a function of the ratio of the peak seed intensity to peak pump intensity. The solid line is the result of the numerical calculations described in Sec. III C, and the dashed line is the result expected from the saturation value obtained from the analytic solutions obtained in Sec. III A.

The amplification factor calculated analytically can be used to obtain the conversion efficiency for weak seed

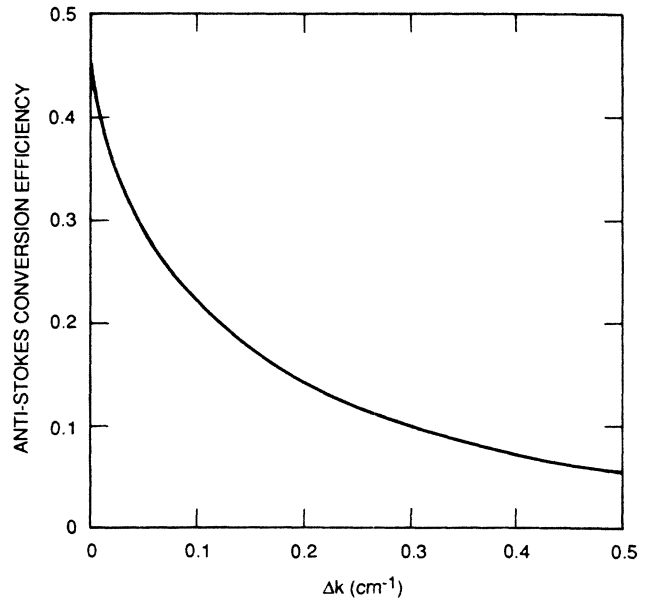

FIG. 6. Anti-Stokes conversion efficiency as a function of the phase mismatch Δk, for the optimum seed strength determined from the maximum of the solid curve in Fig. 5.

pulses when $\Delta k = 0$. For the Gaussian pulses considered, with equal FWHM for pump and seed, the peak intensity ratio λ also gives the ratio of initial energies. For $\lambda \ll 1$, Eqs. (26) then show that the final energy of the Stokes pulse will be a factor of

$$\zeta(\lambda) = \lambda[\omega_1/(2\omega_R)]^2 \tag{37}$$

times larger than the initial energy. If pump depletion is negligible, this value will also give the conversion efficiency. We have plotted this estimate of the conversion efficiency in Fig. 5. For large values of λ, the formula breaks down because of the large amount of energy lost from the pump and also contained in the Stokes wave. Therefore, we truncated the function at the value of λ for which the $\zeta(\lambda) = \frac{1}{3}$, roughly corresponding to an equal division of energy between Stokes, pump, and anti-Stokes waves. This simple approach coincides remarkably well with the value of λ that maximizes the conversion efficiency in a more detailed calculation.

We note two further points about this simple estimated $\zeta(\lambda)$. Equation (37) gives a result somewhat larger than the calculations even for cases when pump depletion is negligible ($\lambda \sim 10^{-3}$). This occurs because the oscillations due to the Bessel functions in Eq. (26) have not fully damped out. We ended the numerical calculations after one meter of propagation. Second, the conversion efficiency predicted by the numerical calculations falls off as λ increases past 1.5%. This regime, of course, is completely beyond the range of the simple formula (37). However, the behavior can be qualitatively understood by noting that for larger seeds, pump depletion will cut off amplification of Stokes and anti-Stokes faster. Since the anti-Stokes is initially zero and must be generated, it attains a smaller final value in those cases.

The results shown in Fig. 6 have important experimental implications. The ideal situation of perfect matching, $\Delta k = 0$, for the pump, Stokes, and anti-Stokes wave vectors corresponds to the vector coupling diagram in Fig. 2. This situation can be achieved by crossing the pump beam and Stokes seed beam at the very small angle θ_{-1}. A typical value of θ_{-1} would be a few milliradians. Changing the crossing angle would increase the minimum possible value of Δk. A simple calculation of the minimum possible Δk for each crossing angle of the initial laser beams leads to the conclusion that this crossing angle must be very accurately achieved. We note, however, that such an estimate might be modified by a more detailed theory that took into account the finite diameter of the beam and possible focusing effects of the beams.

The calculated conversion efficiencies as a function of the distance propagated for three values of Δk are shown in the next series of diagrams. Figures 7 and 8 correspond to the point for $\Delta k = 0$, $\Delta k = 0.2$ cm^{-1}, and $\Delta k = 0.4$ cm^{-1} in Fig. 6. For Fig. 7, we have also included second-order waves ($n = -2$ and $n = 2$). Perfect phase matching for waves $n = -1$, 0, and 1 was assumed, and the wave vectors for the higher-order waves $n = -2$ and $n = 2$ were determined according to the prescription in Sec. II. The other parameters were the same as for the calculation described in Fig. 5. Slightly less frequency conversion to the anti-Stokes wave is observed. For the larger values of Δk used for Fig. 8, the greatly reduced growth of the anti-Stokes waves in the absence of phase matching is clearly exhibited. These calculations included only the Stokes, pump, and anti-Stokes waves.

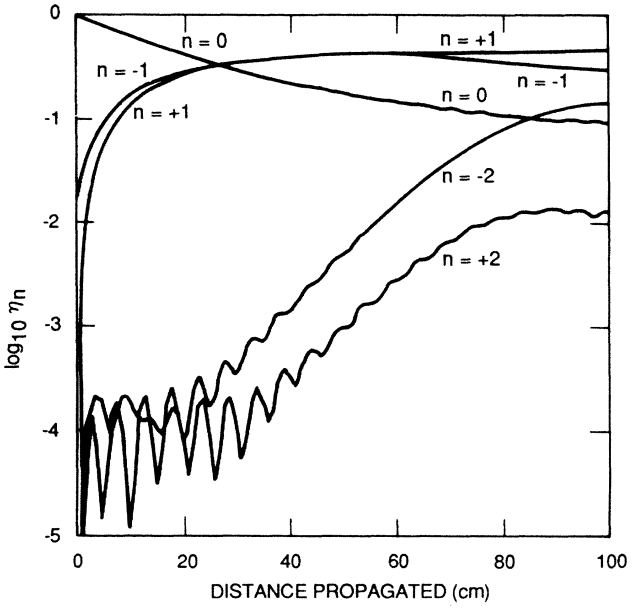

FIG. 7. Conversion efficiency as a function of distance propagated for a calculation at the optimum seed strength and perfect phase matching. The integers label the order of the corresponding waves: 0 is pump, −1 is Stokes, +1 is anti-Stokes, etc. Note the effect of second-order Stokes and anti-Stokes waves.

IV. CONCLUDING REMARKS

We have investigated the interaction of different frequency components in a Raman medium. Analytic and

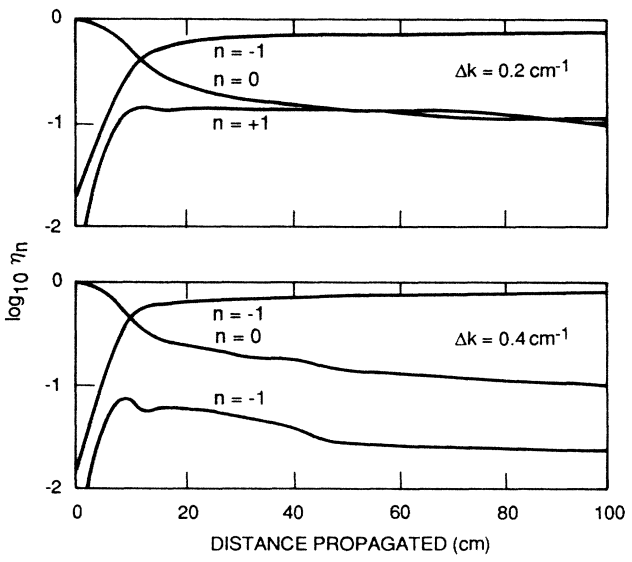

FIG. 8. Conversion efficiency as a function of distance propagated for calculations at the optimum seed strength but with phase mismatch Δk between waves.

numerical solutions of the one-dimensional Maxwell-Bloch equations have been obtained under a variety of circumstances. The emphasis of the work has been to examine the coupling of Stokes, pump, and anti-Stokes pulses as a function of their relative phase matching.

A major result has been the discovery of an analytic solution describing Stokes–anti-Stokes gain suppression in the transient case. We also determined, numerically, a scaling function that predicts the transient gain coefficient for the Stokes gain as a function of the momentum mismatch Δk. The momentum mismatch is determined by the relative angles of the wave vectors describing the propagation of the three pulses. In an experiment Δk can be related to the crossing angle of the pump and seed beams. We will investigate in future work the angular intensity patterns of Stokes and anti-Stokes radiation that would be expected.

We also attempted to find conditions that led to the efficient generation of anti-Stokes radiation. For the cases considered, we observed as much as 40% conversion efficiency to the anti-Stokes. Precise control of the crossing angles between the pump beam and the seed Stokes beam would be required to realize this. However, our estimates are based on solutions to a one-dimensional wave equation. Recent work by Ritchie[5] has shown a reduction of the conversion efficiency when transverse terms in the wave equation are considered. Further theoretical and experimental investigation of anti-Stokes generation is needed.

ACKNOWLEDGMENTS

This work was supported by Sandia National Laboratory and by Lawrence Livermore National Laboratory. One of us (A.P.H.) acknowledges helpful conversations with B. Ritchie.

[1]D. Eimerl, R. S. Hargrove, and J. A. Paisner, Phys. Rev. Lett. **46**, 651 (1981).

[2]J. R. Ackerhalt, Phys. Rev. Lett. **46**, 922 (1981).

[3]A. P. Hickman, J. A. Paisner, and W. K. Bischel, Phys. Rev. A **33**, 1788 (1986).

[4]J. R. Ackerhalt and P. W. Miloni, Phys. Rev. A **33**, 3185 (1986).

[5]B. Ritchie, Phys. Rev. A **35**, 5108 (1987).

[6]V. Wilke and W. Schmidt, Appl. Phys. **16**, 151 (1978); **18**, 177 (1979).

[7]K. Drühl, R. G. Wenzel, and J. L. Carlsten, Phys. Rev. Lett. **51**, 1171 (1983).

[8]N. Bloembergen, *Nonlinear Optics* (Benjamin, Reading, MA, 1977).

[9]M. D. Duncan, R. Mahon, J. Reintjes, and L. L. Tankersley, Opt. Lett. **11**, 803 (1986).

[10]D. J. Brink and D. Proch, J. Opt. Soc. Am. **73**, 23 (1983).

[11]R. L. Carman, F. Shimizue, C. S. Wang, and N. Bloembergen, Phys. Rev. A **2**, 60 (1970).

[12]*Handbook of Mathematical Functions,* edited by M. Abramowitz and I. A. Stegun (U.S. GPO, Washington, D.C., 1968).